Journal Name

ARTICLE TYPE

Cite this: DOI: 10.1039/xxxxxxxxxx

Organic Layer Formation and Sorption of U(VI) on Acetamide Diethylphosphonate-Functionalized Mesoporous Silica†

Eva C. Uribe,*[a] Harris E. Mason,[b] Jennifer A. Shusterman,[b] and Wayne W. Lukens[c]

Received Date
Accepted Date

DOI: 10.1039/xxxxxxxxxx

www.rsc.org/journalname

Acetamide diethylphosphonate (AcPhos)-functionalized silica has been shown to have a high affinity for U(VI) in pH 2-3 nitric acid solutions. Previous work has focused on actinide and lanthanide extraction under various conditions, but has shown poor reproducibility in the functionalization process. For this work, four AcPhos-functionalized SBA-15 materials were synthesized and evaluated based on their U(VI) sorption capacity and their resilience to contact with pH 3 nitric acid solutions. Materials synthesized with a pyridine base catalyst were shown to form a greater fraction of polymeric structures at the silica surface, which correlated with higher structural integrity upon contact with acidic solutions. The single-pulse ^{31}P and ^{1}H NMR spectra of these materials show evidence of the formation of phosphonic acid groups, as well as hydrogen-bonding interactions between ligands or with the silica surface. Additionally, these materials were found to have a significantly higher U(VI) sorption capacity and K_{eq} than the materials synthesized without pyridine, most likely due to the ion-exchange properties of the phosphonic acid groups. The ^{31}P$-^{31}$P DQ-DRENAR NMR technique was used to compare the average strength of dipolar coupling interactions between phosphorus atoms for the four different materials. Because the strength of dipolar coupling interactions depends on the number and proximity of neighboring spins, this technique provides information about the average density of ligands on the surface. The conventional functionalization procedure yielded materials with the lowest average surface ligand density, while those using extended reaction times and the pyridine base catalyst yielded materials with higher surface ligand densities.

Introduction

Ordered mesoporous silica substrates provide ideal backbones for grafting functional groups for the selective extraction of cation species from aqueous, acidic media. The high surface area provides increased interaction area between organic functional groups and aqueous species. Furthermore, they can be synthesized using a simple self-assembly method of alkoxysilanes, which are reactive with surface silanol groups. The reactivity of surface-functionalized materials depends on the extent of surface coverage and the distribution or density of functional groups on the surface. Solid-state nuclear magnetic resonance spectroscopy (NMR) is a powerful tool that can probe the structure of the functional layer. In this study, we use the DQ-DRENAR sequence [1,2] to measure the strength of ^{31}P-^{31}P homonuclear dipolar coupling in four SBA-15 materials functionalized with diethylacetamide phosphonate (AcPhos) using three different functionalization procedures. These studies are combined with conventional solid-state NMR techniques used to assess the stability of functional layer in nitric acid solutions. Ultimately the NMR techniques are used to explain differences in U(VI) sorption observed across the materials.

The AcPhos ligand was adapted from a class of carbamoyl methylphosphine oxide (CMPO) ligands, which are used in solvent extraction for the selective extraction of actinides, primarily trivalent actinides, from the lanthanides. A wealth of literature exists describing the macroscopic extraction of actinides and lanthanides using solid materials grafted with or impregnated with phosphate-based ligands. Horwitz et al. have reported a number of extraction chromatography resins designed for the selective extraction of actinides and rare earths using CMPO and other organophosphorus ligands.[3–5] A variety of phosphinic and phosphoric acid-impregnated resins were tested for extraction of ac-

[a] Department of Chemistry, University of California, Berkeley, Berkeley, California 94720, USA. E-mail: eva.uribe@berkeley.edu
[b] Glenn T. Seaborg Institute, Physical and Life Sciences Directorate, Lawrence Livermore National Laboratory, L-231, PO Box 808, Livermore, California 94550, USA
[c] Chemical Sciences Division, Lawrence Berkeley National Laboratory, 1 Cyclotron Road, Berkeley, California 94720, USA

† Electronic Supplementary Information (ESI) available. See DOI: 10.1039/b000000x/

tinides from acidic media.[6–8] Wei et al.[7] developed a series of extraction chromatography resins by impregnating polymer resins with CMPO, diethylhexyl orthophosphoric acid (HDEHP), and dithiophosphinic acid (Cyanex 301) for the selective extraction of trivalent f-elements from fission products in high level waste. In these reports, an absence of stability of the impregnated resin material was noted.

Several studies examine the use of phosphonic acid-functionalized silica substrates for catalysis and chromatography.[9–11] Nesterenko et al. synthesized and characterized the ion-exchange properties of aminophosphonic acid-modified silica.[12] There have been several investigations of U(VI) extraction using diethylphosphonate-modified mesoporous silica.[13–21] Additionally, Dudarko et al. used phosphonic acid tethered to mesoporous silica for the extraction of trace U(VI) from aqueous solution under mildly basic conditions.[22]

Fryxell et al. report the anchoring of the AcPhos functional group to silica supports as an extension of the sol-gel process.[23–29] These materials, along with their hydrolyzed phosphonic acid versions were also found to have a high affinity for uranyl and plutonyl in pH 2-3 nitric acid solutions. The ester-AcPhos was shown to have high affinity for lanthanides in $NaNO_3$ solutions, with extraction increasing as the pH was increased from 1 to 6.5. Lanthanide extraction was high for the acid-AcPhos materials even from highly acidic solutions.[23] Extraction of U(VI) and Pu(IV) was also measured for both materials.[28] Generally, the kinetics and thermodynamics of sorption were more favorable for the acid-AcPhos materials, though the ester-AcPhos showed high affinity for U(VI) from pH 0.7-4.55 nitric acid solutions, even in the presence of competing ions.[28]

The scope of these studies was generally restricted to evaluating materials based on their macroscopic extraction properties using batch contact experiments. In particular, little attention was given to evaluation of the constitution of the functional layer after the grafting procedure, other than routine NMR analysis. Additionally, little is known about the resilience of functional materials to contact with acidic solutions. Previous work by our research group has shown that the synthetic procedure used for these studies is not highly reproducible, perhaps in part due to the impurities in the reaction mixture used for the synthesis of AcPhos. Thus, materials synthesized the same way yielded vastly different Pu(VI) sorption properties.[30]

To mitigate some of the factors contributing to poor reproducibility of the functionalization process, the materials described in this chapter were synthesized directly from diethyl (2-oxo-2-((3-(triethoxysilyl)propyl)amino)ethyl)phosphonate (Figure 1, which was purchased from Technocomm Ltd. The ligand was synthesized using an alternative synthetic route, which eliminated the need for using the carbonyl diimidazole activator. Thus, it was obtained in its pure form, as indicated by a clean ^1H solution NMR spectrum of the final product.

This work was motivated by the need to understand the surface functionality and the extraction mechanism for organically functionalized silica surfaces on a molecular level. This work was also motivated by the need to obtain a greater understanding of the functionalization process. The extraction of metal cations from

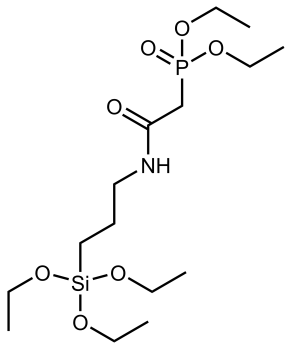

Fig. 1 The acetamide diethylphosphonate ("AcPhos") ligand.

aqueous solutions is affected by not only the extent of loading and the stability of the functional layer, but also by the relative proximity and posture of ligands. Silica gel materials are amorphous on a macroscopic level, but possess short-range, local order. This makes them inaccessible to diffraction methods that rely on long-range order to make structural determinations. For this reason, NMR spectroscopy is ideal for the study of functional layers on mesoporous materials.

There are several reports in the literature that discuss of the structural features of phosphonate- and phosphonic acid-functionalized silica using NMR spectroscopy. Pan et al. and Bibent et al. have conducted in-depth NMR studies on the surface of diethylphosphonate- and phosphonic acid-modified silica and found evidence that the ligands engage in hydrogen bonding interactions.[31,32] Very few have used solid-state NMR spectroscopy to examine the extracted metal-ligand-silica complex formed. Shusterman et al. conducted the first study of the binding mechanism of metal sorption on functionalized silica via NMR spectroscopy on the metal nuclei.[33] In the present work, we combine macroscopic batch contact experiments in aqueous U(VI) solutions with extensive material characterization via NMR spectroscopy, which provides direct, spectroscopic insight into the organic layer formation during functionalization and the interaction with U(VI) species with the functional layer. The AcPhos ligand provides an excellent opportunity to study the functionalization process, and the stability of functional layers in contact with acidic solutions. Because AcPhos-functionalized silica possesses ^1H, ^{31}P, ^{13}C and ^{29}Si, all of which are spin = 1/2 nuclei observable by NMR, and the first two of which are 100% abundant, it is highly accessible to in-depth study by magnetic resonance techniques. Furthermore, as the optimal extraction conditions for U(VI) have been previously optimized, various functionalization procedures can be compared by their ability to extract U(VI) from nitric acid media.

Experimental Methods

Synthesis and Functionalization Procedure.

The SBA-15 rod-shaped particles were synthesized using the hydrothermal method described by Sayari, Han, and Yang,[34] which is described in detail in the ESI†. Silica particles were functionalized directly using diethyl (2-oxo-2-((3-(triethoxysilyl)propyl)amino)ethyl) phosphonate, "AcPhos" (Fig-

ure 1) using a method adapted from the surface polymerization method described by Sander.[35] Four materials, AcPhos-SBA (1-4) were synthesized using three different functionalization procedures. All functionalization procedures involved drying of the silica particles under vacuum overnight followed by the addition of toluene and water (and pyridine, for AcPhos-SBA (3) and (4)) under a nitrogen atmosphere. After surface hydration, the AcPhos ligand was added, and the reaction mixture refluxed for a given reaction time. After a distillation step to remove excess water and ethanol evolved during the reaction, solid materials were collected via vacuum filtration, washed with isopropanol, and stored in an evacuated desiccator. Additional synthetic details are given in the ESI†. The key differences between synthetic procedures for AcPhos-SBA (1-4) are summarized in Table 1. The resulting non-functionalized SBA and AcPhos-SBA materials were characterized for surface area and porosity using nitrogen adsorption isotherms.

Nitrogen Adsorption Isotherm Measurement.

Nitrogen adsorption measurements were performed on a Micromeritics Accelerated Surface Area and Porosity (ASAP) 2420 System instrument. For a typical measurement, 30 mg of solid material was transferred to a pre-weighed glass tube under nitrogen and outgassed for 24 hours. The sample was then reweighed. Nitrogen isotherms at 77 K were performed in liquid nitrogen baths using ultra-high purity gas. Additional details are given in the ESI†. The average surface area per gram of material was determined using the Brunauer-Emmett-Teller (BET) method,[36] and average pore volume and pore diameter were obtained using the Barrett-Joyner-Halenda (BJH) method.[37]

Batch Contact Experiments.

A ^{233}U radiotracer was used for all batch contact experiments due to its high specific alpha activity. Details on the ^{233}U stock purification procedure are provided in the ESI†. For measurement of U(VI) sorption isotherms, samples with U(VI) concentrations higher than 20 μM were prepared using a mixture of ^{233}U and depleted ^{238}U stocks. The depleted ^{238}U stock was prepared by dissolution of $UO_2(NO_3)_2 \cdot 6H_2O$ (Sigma Aldrich) in 1 M HNO_3.

Prior to contact with U(VI) stocks, solid samples were pre-equilibrated in solution for approximately 15 hours in a ratio of 1 mg solid mL^{-1} solution. Samples were then spiked with U(VI) stocks to achieve the desired U(VI) concentration, and the pH readjusted using NaOH. Centrifugation at 7000 rpm (8765 *g*) achieved phase separation, and 10 μL aliquots were taken for liquid scintillation counting. Samples were typically assayed after 1, 4, and 24 hours, though in every case, additional sorption was not observed after 1 hour mixing time. In between assays, samples were gently rocked on a rotoshake. For samples at pH 2 and 3, the pH was measured and adjusted after each asasy. To measure the dependence of U(VI) sorption on [HNO_3], samples were prepared with an initial concentration of [^{233}U(VI)] = 2×10^{-5} M, in solutions containing 3 M, 2 M, 1 M, pH 1, pH 2, and pH 3 nitric acid. Additionally, sorption of U(VI) was compared at pH 2 and pH 3 for samples containing no additional $NaNO_3$ and 3 M $NaNO_3$. These samples contained an initial [U(VI)] = 500 μM, comprised of [^{233}U(VI)] = 20 μM as a tracer and [^{238}U(VI)] =480 μM.

U(VI) sorption isotherms were measured for non-functionalized SBA, AcPhos-SBA (2), AcPhos-SBA (3), and AcPhos-SBA (4) from 3 M $NaNO_3$ solutions adjusted to pH 3. Solid samples were pre-equilibrated with solution in a ratio of 1 mg solid mL^{-1} solution for approximately 15 hours. Samples were then spiked with U(VI) stocks to obtain initial concentrations of [$U(VI)_{total}$] = 20, 50, 100, 200, 300, 400, and 500 μM. For each sample, the [^{233}U] = 20 μM. Samples were rocked continuously. After 1, 4, and 24 hours of mixing time, samples were centrifuged at 7000 rpm, and 10 μL assays were taken for liquid scintillation counting of the ^{233}U alpha activity. No additional sorption was observed after 1 hour of mixing time. A control sample containing no solid and $[U(VI)]_{total}$ = 500 μM was assayed with the samples to verify that no uranyl species precipitated or adsorbed to the polypropylene tube walls.

NMR Sample Preparation and Instrumentation.

U(VI)-AcPhos-SBA (2, 3, and 4) samples were prepared using conditions similar to those tested in the U(VI) isotherm measurements, in 3 M $NaNO_3$ adjusted to pH 3. After pre-equilibration, samples were spiked with only ^{238}U stock to achieve an initial concentration of 5×10^{-4} M. After mixing for 24 hours, samples were centrifuged at 7000 rpm, and the supernatant withdrawn. Samples were washed with approximately 100 μL fresh 3 M $NaNO_3$ adjusted to pH 3 and then air dried in a fume hood prior to packing into Kel-F rotor inserts.

Acid-washed AcPhos-SBA samples, denoted AcPhos-SBA (X) AW, where X is 1, 2, 3, and 4 were prepared by contacting each material with 3 M $NaNO_3$ adjusted to pH 3 for approximately 20 hours. Approximately 50 mg of solid sample was washed with 10 mL of solution. As usual, the phases were separated by centrifugation. The supernatant was withdrawn, and each sample was washed with 2-3 mL isopropanol to rinse excess water away from the surface. This was repeated twice. Finally, the samples were air-dried, collected in glass vials, and placed in a desiccator evacuated to less than 20 mtorr Hg for 7 hours. Finally, samples were stored in the same evacuated desiccator as pristine samples to achieve similar levels of surface hydration.

Ligand content for the pristine and acid-washed materials was determined via single-pulse ^{31}P NMR measurements of samples containing hydroxyapatite as an internal standard. To prepare each sample, the AcPhos-SBA material and hydroxyapatite were weighed separately, ground together to achieve homogeneity, and transferred to a pre-weighed NMR rotor. The pulse delay was 60 s. All solid-state NMR spectra were collected on a 300 MHz (7.5 T) Tecmag Apollo with a Bruker HX CP/MAS probe configured for 4 mm (o.d.) rotors. Operating frequencies were 59.82, 75.73, 301.13, and 121.90 MHz for ^{29}Si, ^{13}C, ^{1}H, and ^{31}P, respectively. For ^{31}P single-pulse and all cross-polarized spectra, the magic angle spinning (MAS) rate was 10 kHz. All DQ-DRENAR data were collected at a MAS rate of 7 kHz. The single-pulse ^{1}H spectra were collected using a MAS rate of 13 kHz. Chemical

Table 1 Summary of the difference in synthetic procedures for the AcPhos-SBA materials

Material	AcPhos-SBA (1)	AcPhos-SBA (2)	AcPhos-SBA (3)	AcPhos-SBA (4)
Surface hydration (H_2O molecules nm^{-2})	10	10	10	10
Surface hydration time (hours)	2	15	15	15
Catalyst used (molecules nm^{-2})	N/A	N/A	5	5
Silanes added (silanes nm^{-2})	6.25	6.25	6.25	6.25
Reflux time (hours)	6	24	24	24

shifts were referenced using secondary references as follows: ^{13}C using glycine (δ_C = 42.8 and 173.6 ppm from tetramethylsilane TMS),[38] ^{29}Si using kaolinite (δ_{Si} = -91.5 ppm from TMS),[39] ^{31}P using hydroxyapatite (δ_P = 2.65 ppm from 85% H_3PO_4),[40] and ^{1}H using hydroxyapatite (δ_H = 0.2 ppm from TMS).[41] Spectra were deconvoluted using the open source software Peak-O-Mat. All spectral resonances were fitted using pseudo-Voigt functions to determine integrated peak areas.

^{31}P single-pulse magic angle spinning (SP/MAS) spectra were collected using a pulse delay of 60 s, and a pulse width of INSERT X. Where noted, continuous wave (CW) decoupling was applied on the ^{1}H channel during acquisition. The single pulse ^{1}H spectra were collected using a $\pi/2$ pulse width of 7.3 μs, a π pulse width of 14.6 μs, and a pulse delay of 2 s. The sequence used to collect single-pulse ^{1}H spectra was modified using π pulses in order to decrease the background from protons outside the sample. ^{29}Si cross-polarization magic angle spinning (CP/MAS) spectra were collected using a 2 s pulse delay and a 3 ms (CW) polarization transfer. ^{13}C CP/MAS spectra were collected using a 2 s pulse delay and a 1 ms ramped amplitude polarization transfer on the ^{13}C channel, with CW decoupling on the ^{1}H channel during signal acquisition.

$^{31}P-^{31}P$ Double-Quantum-based Dipolar recoupling effects Nuclear Alignment Reduction (DQ-DRENAR)[1,2] measurements were made using a series of rotor-synchronized POST-C7 pulse sequences, with a $\pi/2$ pulse width of 5.1 μs, a 2π pulse width of 20.4 μs, and a $3\pi/2$ pulse width of 15.3 μs. The amplitude of the pulses was adjusted such that the desired pulse sequence could be completed in two rotor cycles. Spectra were acquired after the application of two POST-C7 pulse sequences n times, where n is an integer number between 1 and 10. Therefore, signal was acquired after ten different "signal evolution times" ranging from NT_r = 0.57 to 5.7 ms where N is an integer number of rotor periods (always a multiple of four) and T_r is the rotor period. For the control experiment, the second POST-C7 pulse sequence is out of phase by $\pi/2$, which prevents dipolar recoupling.

Results

Characterization by N_2 Adsorption.

Table 2 summarizes the nitrogen adsorption isotherm data obtained for non-functionalized SBA-15 and the four AcPhos-SBA materials. The adsorption data and the pore size distribution and cumulative pore volume data for non-functionalized SBA is shown in Figure S1†. Corresponding data for the AcPhos-SBA materials are shown in Figures S2-S5. The non-functionalized material demonstrates the highest specific surface area, specific pore volume, and pore diameter. Its isotherm is consistent with a type IV isotherm with an H_1 hysteresis loop, which is consistent with capillary condensation in a highly ordered, cylindrical mesoporous structure.[42]

AcPhos-SBA (1) demonstrates similar isotherm shape and pore diameter, indicating that ligand grafting has not significantly altered the pore structure. The specific surface area and specific pore volume have decreased, which is consistent with an increase in mass that results from functionalization. This was also observed for the other AcPhos-SBA materials, especially AcPhos-SBA (3) and (4), which indicates that these materials have the highest ligand loading of all the materials. AcPhos-SBA (2), (3), and (4) show a more significant decrease in average pore diameter than does AcPhos-SBA (1) compared to the non-functionalized material. Similar 1-3 nm decreases in average pore diameter have been observed in other silica materials after modification with an organic monolayer.[21,43,44]

While the nitrogen adsorption isotherms of AcPhos-SBA (1) and (2) are both type IV with H_1 hysteresis loops, the shapes of the isotherms for AcPhos-SBA (3) and (4) look different. The isotherm and hysteresis loop for AcPhos-SBA (3) appear to be type IV-H_1. However, there is also hysteresis in the desorption branch at low and high partial pressures (Figure **??**). The hysteresis loop in the isotherm of AcPhos-SBA (4) may be a hybrid between H_2 and H_4 isotherms, which are most often associated with disordered pore structures with bottle-neck or slit-shaped openings.[42] However, both of these phenomena, desorption hysteresis and similar changes in hysteresis loop shape, have been observed for organically-modified materials when the number of adsorption sites changes with increasing partial pressure of the nitrogen during isotherm measurement.[45] Therefore, the hysteresis loop shapes of AcPhos-SBA (3) and (4) does not necessarily indicate a significant change in pore ordering and structure.

^{13}C and ^{29}Si NMR Spectroscopy.

$^{13}C\{^{1}H\}$ CP/MAS spectra were collected for the four AcPhos-SBA materials in their as-synthesized, pristine state, as well as after washing them with pH 3 nitric acid solutions containing 3 M $NaNO_3$. These conditions were chosen to match those used in the measurement of the U(VI) sorption isotherms. Spectra of pristine and acid-washed samples were compared in order to verify ligand structure and to qualitatively assess resiliency of the ligand structure to contact with acid for each material. The AcPhos ligand contains nine distinct carbon sites. As two of these sites have similar chemical shifts, eight resonances are observed in the $^{13}C\{^{1}H\}$ CP/MAS spectra of all pristine and acid-washed samples. The observed resonances are assigned as follows: δ_C = 8.0 ppm ($-Si-\mathbf{C}H_2-CH_2-$), 14.0 ppm ($0=P-O-CH_2-\mathbf{C}H_3$), 21.7 ppm ($-Si-O-CH_2-\mathbf{C}H_3$), 33.4 ppm ($-Si-CH_2-\mathbf{C}H_2-CH_2-NH-$),

Table 2 Summary of N_2 adsorption isotherm data for AcPhos-SBA materials

Material	BET Surface Area ($m^2\ g^{-1}$)	BJH Pore Volume ($cm^3\ g^{-1}$)	BJH Pore Diameter (nm)	Hysteresis Loop Type
SBA-15	831	0.818	7.47	H_1
AcPhos-SBA (1)	442	0.536	7.42	H_1
AcPhos-SBA (2)	383	0.450	6.43	H_1
AcPhos-SBA (3)	125	0.128	4.32	H_1 with desorption hysteresis
AcPhos-SBA (4)	46	0.045	4.32	H_2 or H_4

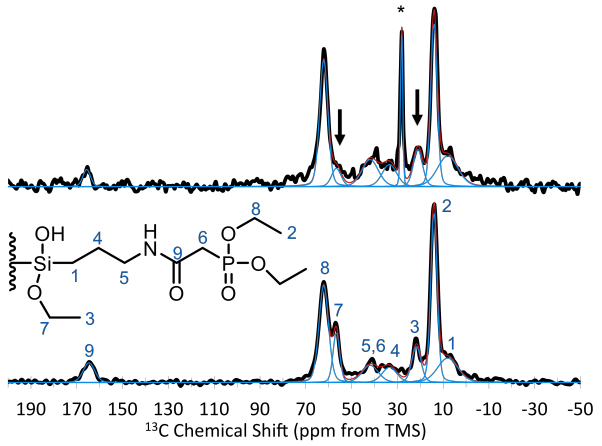

Fig. 2 $^{13}C\{^1H\}$ CP/MAS spectra for AcPhos-SBA (1) pristine (bottom) and acid-washed (top). Spectra were normalized to the peak at 14 ppm. The black arrows point to the resonances at 21.7 and 56.6 ppm, which correspond to the carbons on the ethoxy groups of the siloxane. Surface-sorbed isopropanol gives rise to a narrow peak at 28.1 ppm, labeled with an asterisk in the figure.

41.8 ppm (mixture of $-CH_2-\mathbf{C}H_2-NH-$ and $-CO-\mathbf{C}H_2-P=0$), 56.6 ppm ($-Si-O-\mathbf{C}H_2-CH_3$), 62.2 ppm ($O=P-O-\mathbf{C}H_2-CH_3$), and 164.7 ppm ($-\mathbf{C}=O$). These chemical shift values are largely consistent with the values reported by Fryxell et al.[23] for MCM-41 materials grafted with the ester AcPhos functional group, with the exception that they assume that all siloxane esters are hydrolyzed during functionalization. In the present work, this assumption is not made, and there is evidence that these groups are still present, as discussed below. Figure 2 shows the spectra for the pristine and acid-washed samples of AcPhos-SBA (1). The additional very sharp peak appearing in the spectrum for AcPhos-SBA (1) AW at 28.1 ppm with respect to TMS is believed to be from surface-sorbed isopropanol, which was used in washing the samples. Corresponding spectra for AcPhos-SBA (2), (3), and (4) are shown in Figures S6-S8.

The ^{13}C NMR spectra were collected using cross-polarization from ^1H. Because of the difference in polarization transfer kinetics for the different carbon species, the integrated peak areas are not proportional to the populations of their corresponding carbon atoms. Additionally, differences in the amount of water adsorbed to the pristine versus acid-washed samples may result in different CP dynamics. This difference was minimized by drying the acid-washed samples under vacuum ($< 20\ \mu$m Hg) for several hours. Therefore, differences in the relative peak amplitude for two spectra may indicate structural changes to the AcPhos ligand.

The $^{13}C\{^1H\}$ CP/MAS spectrum for pristine AcPhos-SBA (2) looks similar to that of AcPhos-SBA (1). Comparison of the spectra for pristine and acid-washed AcPhos-SBA (2) shows significant decrease in peak amplitudes at the C_3 and C_7 positions (black arrows in Figure S6†). These changes are consistent with hydrolysis of ethoxy groups from the silane upon contact with acidic media. Similar differences can be observed upon comparing the pristine spectra for AcPhos-SBA (1) and (2) with those of AcPhos-SBA (3) and (4). In contrast to AcPhos-SBA (1) and (2), the acid-washed spectra are nearly identical to the pristine spectra for both AcPhos-SBA (3) and (4).

Figure 3 shows the $^{29}Si\{^1H\}$ CP/MAS spectra for pristine and acid-washed AcPhos-SBA (1). Corresponding spectra for AcPhos-SBA (2), (3), and (4) are shown in Figures S9-S11. The ^{29}Si NMR spectra for silica typically has three spectral resonances. These are named Q^n, for the species $SiO_n(OH)_{4-n}$. The Q^4, Q^3, and Q^2 species are SiO_4, $SiO_3(OH)$, and $SiO_2(OH)_2$, and give rise to peaks at approximately -110.2, -101.9, and -90.8 ppm, with respect to TMS, respectively. These chemical shift values are consistent with previous reports.[46,47] The amplitude of peaks from surface silicon atoms is enhanced in cross-polarized spectra due to their proximity to ^1H. Upon functionalization, some of the surface silanols are replaced by siloxanes, which give rise to a second group of resonances between approximately -49 and -70 ppm. These are the T^m species, corresponding to $RSiO_m(OX)_{3-m}$, where R is the organofunctional group and X is H or an alkoxy group. When water is used during functionalization, the T^1, T^2, and T^3 resonances are usually interpreted as corresponding to isolated ligand monomers, dimers or polymer chain terminals, and more extended polymer networks, respectively. In principle, similar chemical shifts appear for siloxanes which form one, two, or three covalent bonds to surface silanols. In the spectra reported here, the T^1, T^2, and T^3 resonances are observed at -49.7, -57.7, and -66.6 ppm, with respect to TMS, respectively. These chemical shift values are also consistent with previous reports.[48,49]

As these spectra were also collected using cross-polarization, the integrated peak areas cannot be used to quantify the different species. However, since they were collected under identical conditions, the relative peak ratios between samples can be compared to characterize the functional layer qualitatively. Table 3 summarizes the percent areas for the T and Q peaks for all four pristine and acid-washed samples.

In comparing the pristine materials, it can be seen that AcPhos-SBA (3) and (4) are very similar to each other. Unlike the spectra for AcPhos-SBA (1) and (2), those of AcPhos-SBA (3) and (4) have a significant T^3 peak, and the T^2 peaks make a up a much larger percentage of the functionalized silicon atoms. Compared to AcPhos-SBA (3) and (4), AcPhos-SBA (1) and (2) have a larger relative population of Q^2 and Q^3 Si atoms, which is consistent

Table 3 Comparison of peak ratios for AcPhos-SBA ^{29}Si{^{1}H} CP/MAS spectra

Material	T^1/T	T^2/T	T^3/T	Q^2/Q	Q^3/Q
AcPhos-SBA (1)	0.82	0.18	0	0.06	0.41
AcPhos-SBA (1) AW	0.24	0.76	0	0.08	0.46
AcPhos-SBA (2)	0.78	0.22	0	0.04	0.37
AcPhos-SBA (2) AW	0.41	0.59	0	0.04	0.43
AcPhos-SBA (3)	0.12	0.71	0.17	0.1	0.44
AcPhos-SBA (3) AW	0.12	0.70	0.17	0	0.43
AcPhos-SBA (4)	0.09	0.74	0.18	0.1	0.44
AcPhos-SBA (4) AW	0.01	0.74	0.25	0	0.43

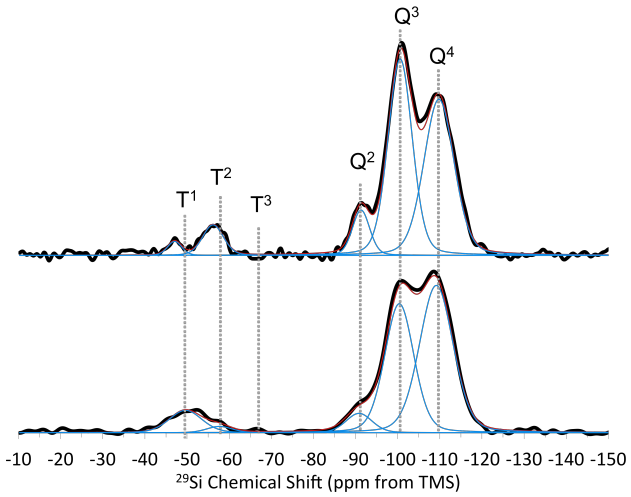

Fig. 3 ^{29}Si{^{1}H} CP/MAS spectra for AcPhos-SBA (1) pristine (bottom) and acid-washed (top). Spectra were normalized to the peak at -109 ppm. Experimental data is shown in black. The blue lines show the spectral deconvolution, and the red line is their sum. Gray dashed lines mark the positions of the Q^n and T^m peaks.

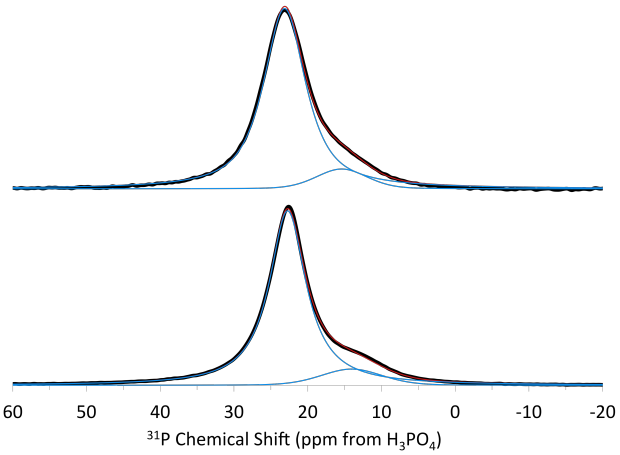

Fig. 4 ^{31}P single-pulse MAS spectra for AcPhos-SBA (4) pristine (bottom) and acid-washed (top). Spectra were normalized to the single peak at 22.7 ppm. Experimental data is shown in black, and the red line is the spectral fit. No ^{1}H decoupling was used in the collection of these spectra. The corresponding spectra for AcPhos-SBA (3) are shown in Figure S14†.

with higher surface silanol content. Pristine AcPhos-SBA (2) has a slightly higher percentage of T^2 and a slightly lower percentage of Q^3 compared to pristine AcPhos-SBA (1). Qualitative comparison of the spectra and the peak ratios in Table 3 shows that in general the structure of the functional layer does not change upon contact with acidic solutions for AcPhos-SBA (3) and (4), but it changes significantly for AcPhos-SBA (1) and (2). For both AcPhos-SBA (1) and (2), the T^1 peak amplitude is diminished, and the the Q^3:Q ratio has increased significantly, which again indicates that the silanol content has increased upon contact with acid.

Single-Pulse ^{31}P NMR Spectroscopy

^{31}P single-pulse (SP) MAS NMR spectra for AcPhos-SBA (1) and (2) show a single resonance around 23 ppm with respect to H_3PO_4. This indicates that there is only one type of chemical environment for the acetamide phosphonates on the surface. The chemical shift and peak shape do not change after contact with acid for these materials. Their spectra are shown in Figure S12-S13†.

The ^{31}P SP/MAS NMR spectra for AcPhos-SBA (3) and (4) are more complicated, though they are very similar to one another and do not appreciably vary between the pristine and acid-washed samples. As Figure 4 shows, each of these spectra show two distinct resonances: one around 23.0 ppm and one at approximately 15 ppm.

Similar observations have been made for silica functionalized with phosphonic acid ligands.[31,32,50–52] These studies have attributed the lower chemical shift peak to hydrogen bonding interactions, though there is some disagreement in the literature about the assignment of this peak. A phosphonic acid group involved in hydrogen bonding can act as either a hydrogen bond donor through P−OH or as hydrogen-bond acceptors through O=P. Bibent et al.[32] argue that only the second interaction would involve a significant change int he local electron density of the phosphorus atom, resulting in a chemical shift. However, if O=P acts as a hydrogen bond acceptor, it will serve to de-shield the phosphorus atom, resulting in a chemical shift in the opposite direction (towards higher chemical shift value). Pan et al.[31] make the opposite assignment and argue that the lower chemical shift peak is due to phosphonic acid serving as a hydrogen bond donor. Yang et al.[53] conducted ^{31}P NMR measurements on dimethyl methylphosphonate (DMMP) and its hydrolysis products. They observe a chemical shift of δ_P = 36.8 ppm for DMMP and of δ_P = 32.6 ppm and 29.2 ppm for the first and second hydrolysis products, respectively. Broad peaks observed between 20 and 30 ppm are assigned to hydrolyzed, deprotonated methylphosphonate.

Therefore in the present work, the peak observed at 23 ppm in AcPhos-SBA (3) and (4) are likely a mixture of diethyl phos-

phonate P−OEt and hydrolyzed phosphonic acid groups P−OH. The resonance appearing at a chemical shift of 15 ppm is assigned to deprotonated phosphonic acid groups P−O$^-$, which may then be involved in hydrogen-bonding interactions of the type P−O−H−O−P.

Ligand Quantification using Hydroxyapatite and Single-Pulse ^{31}P.

The amount of ligand loaded onto the surface was determined for each pristine and acid-washed material using single-pulse ^{31}P NMR spectroscopy. Each material was ground together with hydroxyapatite, which has a chemical shift of $\delta_P = 2.65$ ppm from 85% H_3PO_4.[40] For single-pulse spectra, the integrated peak area is proportional to the number of phosphorus atoms in each chemical shift environment. Thus, by knowing the mass of hydroxyapatite and the mass of AcPhos-SBA loaded into the rotor, the relative peak areas can be used to calculate the number of ligands per gram of material. Table 4 summarizes the results.

Table 4 Ligand quantification using hydroxyapatite and ^{31}P NMR

Material	Ligand Content (mmol/g)
AcPhos-SBA (1)	0.79
AcPhos-SBA (1) AW	0.58
AcPhos-SBA (2)	1.01
AcPhos-SBA (2) AW	0.66
AcPhos-SBA (3)	1.73
AcPhos-SBA (3) AW	1.03
AcPhos-SBA (4)	1.78
AcPhos-SBA (4) AW	1.19

Comparison of Ligand Distribution.

In previous work[21] ^{31}P-^{31}P homonuclear dipolar coupling measurements via the DQ-DRENAR (Double-Quantum-based Dipolar Recoupling effects Nuclear Alignment Reduction)[1,2] were used to assess the density of the functional layer for diethylphosphoatoethyl-functionalized SBA-15. The DQ-DRENAR method consists of two experiments. In the S' experiment, a series of POST-C7 pulse sequences is applied to achieve recoupling between ^{31}P nuclei, which results in a decrease in signal amplitude. The control S_0 experiment applies the same POST-C7 pulse sequences, but they are out of phase by 90 °, which prevents recoupling. The difference in signal amplitude, $\Delta S = S_0 - S'$ can be related to the dipolar coupling constant through:

$$\frac{S_0 - S'}{S_0} = \frac{0.86\pi^2}{15} \cdot b_{jk}^2 \cdot (NT_r)^2 \qquad (1)$$

where b_{jk} is the dipolar coupling constant between two spins j and k. Ren and Eckert[1,2] show that this method can be extended to multi-spin systems with a distribution of pair-wise dipolar coupling constants, characterized by the sum of all pair-wise dipolar coupling interactions, $\sum_{j<k} b_{jk}^2$.

Figure 5 shows the DQ-DRENAR data for the four AcPhos-SBA materials. For AcPhos-SBA (3) and (4), the integrated peak area for the 23 ppm resonance was used to calculate $\Delta S/S_0$. Figure 6 compares the $\Delta S/S_0$ versus NT_r curves for the 23 ppm peak and the 15 ppm peak of AcPhos-SBA (4). The data points shown in

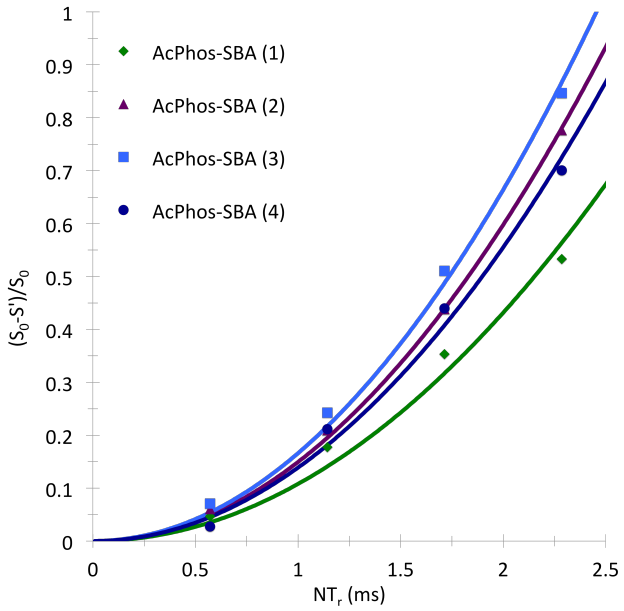

Fig. 5 DQ-DRENAR data for AcPhos-SBA (1), (2), (3), and (4), acquired at a MAS rate of 7 kHz. For AcPhos-SBA (3) and (4), the integrated peak area for the 23 ppm resonances was used to calculate $\Delta S/S_0$.

Figures 5 and 6 were fit with parabolic functions to extract the $\sum_{j<k} b_{jk}^2$ values for each material, which are summarized in Table 5.

Table 5 Dipolar coupling constants measured for AcPhos-SBA using DQ-DRENAR

Material	$\sum_{j<k} b_{jk}^2 (Hz^2 \times 10^5)$
AcPhos-SBA (1)	1.9 ± 0.1
AcPhos-SBA (2)	2.64 ± 0.03
AcPhos-SBA (3) (23 ppm)	2.93 ± 0.07
AcPhos-SBA (4) (23 ppm)	2.45 ± 0.09
AcPhos-SBA (4) (15 ppm)	5.7 ± 0.3

AcPhos-SBA (1) demonstrated the lowest dipolar coupling strength, while those of AcPhos-SBA (2), (3), and (4) are higher. A higher ^{31}P-^{31}P dipolar coupling constant indicates a higher average density of phosphonate groups on the surface. Therefore, AcPhos-SBA (1) has the lowest average density, and AcPhos-SBA (2), (3), and (4) have a higher average density of functional groups. For AcPhos-SBA (4), the phosphorus environment corresponding to the peak at 15 ppm demonstrates stronger dipolar coupling than that at 23 ppm. Therefore, the high dipolar coupling constant calculated for the 15 ppm phosphorus environment shows that it has the highest density of phosphonate groups of all materials measured.

Batch Contact Experiments with U(VI).

The ability of each AcPhos-SBA material to extract U(VI) from various nitric acid media was compared in a series of batch contact experiments. These experiments were conducted both to compare the materials' performance in extraction of uranyl ions from solution, but also to determine ideal conditions for obtaining the maximum amount of U(VI) loaded onto the samples, which

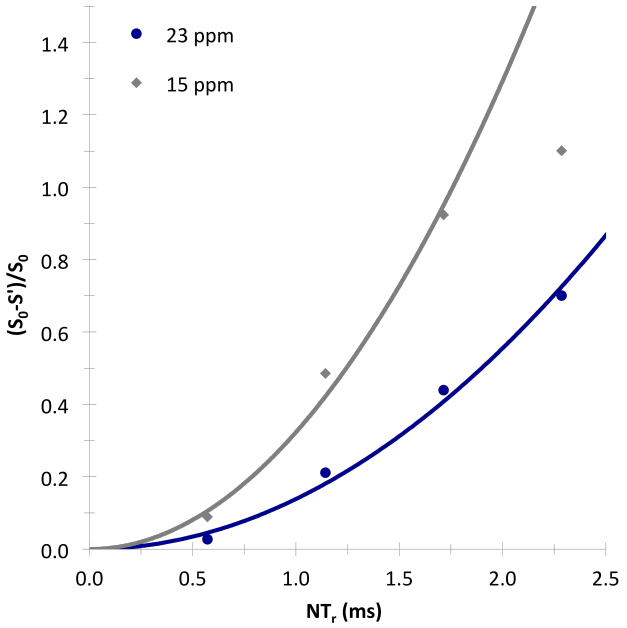

Fig. 6 DQ-DRENAR data for the 23 ppm (blue circles) and 15 ppm (grey diamonds) resonances of AcPhos-SBA(4).

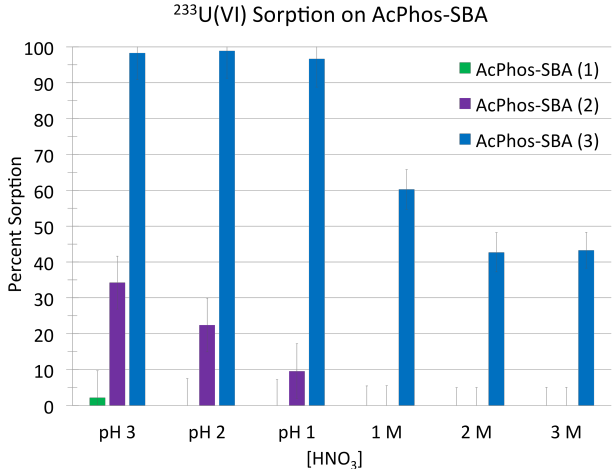

Fig. 7 Percent sorption of ^{233}U(VI) by AcPhos-SBA materials as a function of nitric acid concentration. The initial concentration of U(VI) in solution was 2×10^{-5} M. No additional salts were added to control for ionic strength. The data points shown represent sorption after 1 hour of mixing time.

was necessary for preparation of NMR samples. Figure 7 compares the percent sorption of U(VI) from various concentrations of nitric acid for AcPhos-SBA (1), (2), and (3). The sorption behavior varies widely among the materials. AcPhos-SBA (1) does not extract any significant quantity of U(VI) under any conditions tested. AcPhos-SBA (2) performs slightly better at the lower acid concentrations. It sorbed up to 34% of uranyl present in solution at pH 3. However, at acid concentrations higher than 0.1 M, AcPhos-SBA (2) also did not extract any measurable amount of U(VI) from solution. In contrast, AcPhos-SBA (3) sorbed significant quantities of U(VI) in all conditions tested, including greater than 95% from solutions between pH 1 and 3, and greater than 40% from solutions with nitric acid concentrations between 1 and 3 M.

Previous work[21] showed that increasing the ionic strength resulted in an increase in extraction of U(VI) from nitric acid solutions by phosphonate-functionalized SBA-15. Therefore, sorption of U(VI) from pH 2 and pH 3 solutions containing no additional salt and 3 M $NaNO_3$ was compared for AcPhos-SBA (2), (3), and (4). Figure S14†summarizes the results. At pH 2, both AcPhos-SBA (3) and (4) demonstrate slightly higher sorption of U(VI) at high ionic strength compared to that at low ionic strength. However, the difference is small, and is within the uncertainly of the measurement for AcPhos-SBA (3). At pH 3, the differences are more significant. The amount of U(VI) extracted from high ionic strength solutions is nearly double the amount at low ionic strength for both AcPhos-SBA (3) and (4). Under these conditions, this difference amounts to an additional 75 μmol sorbed U(VI) g^{-1} silica. For this reason, these conditions were chosen for measurement of the U(VI) sorption isotherms, as well as preparation of U(VI) and acid-washed NMR samples.

The U(VI) sorption isotherms for non-functionalized SBA, AcPhos-SBA (2), (3), and (4) were measured for pH 3 solutions containing 3 M $NaNO_3$. The resulting curves were linearized and fit with both the Langmuir and Freundlich sorption isotherm models. The Langmuir isotherm describes monolayer sorption to uniform binding sites, all with equal binding energy. In contrast, the Freundlich isotherm describes sorption to heterogeneous binding sites with a distribution of binding energies. The linearized form of each model used to fit these data are given in ESI†. These fits are shown in Figures 8 and 9. The parameters extracted from the data are summarized in Table 6.

The isotherms of AcPhos-SBA (3) and (4) were better described by the Langmuir model, while that of non-functionalized SBA was better described by the Freundlich model. Both models provided a mediocre fit for the isotherm of AcPhos-SBA (2). AcPhos-SBA (3) and (4) had much higher sorption capacities than AcPhos-SBA (2). The sorption capacities and equilibrium constants calculated for AcPhos-SBA (3) and (4) were the same within the uncertainty of the fit. While the sorption capacity calculated for AcPhos-SBA (2) was similar to that of non-functionalized SBA, the equilibrium constant was much higher, indicating a more stable complex formed with U(VI). The Freundlich model is consistent with sorption to amorphous silica, which has many different types and geometries of binding interactions with a distribution of binding energies.

^{31}P NMR Spectroscopy of U(VI)-AcPhos-SBA Samples.

The single-pulse ^{31}P NMR spectra for U(VI)-AcPhos-SBA (2), (3), and (4) are presented in Figure 10. Each of the spectra demonstrate three resonances, and the fit parameters for each peak deconvolution are reported in Table 7.

The peak shapes and widths of the U(VI)-AcPhos-SBA samples are quite different from their pristine and acid-washed counterparts. For all three sample types (pristine, acid-washed, and U(VI)-contacted), AcPhos-SBA (3) and (4) are very similar. In-

Table 6 Langmuir and Freundlich fit parameters for U(VI) isotherms on AcPhos-SBA

Material	Langmuir Isotherm Model		Freundlich Isotherm Model	
	q_m (μmol g^{-1})	K_{eq} (mL μmol^{-1})	K_F (μmol$^{(1-1/n)}$ mL$^{1/n}$ g^{-1})	n
SBA	140 ± 276	1 ± 1	64 ± 16	1.1 ± 0.1
AcPhos-SBA (2)	37 ± 7	11 ± 5	42 ± 12	2.6 ± 0.7
AcPhos-SBA (3)	157 ± 3	119 ± 50	250 ± 58	3.5 ± 0.6
AcPhos-SBA (4)	162 ± 3	114 ± 41	256 ± 81	3.4 ± 0.9

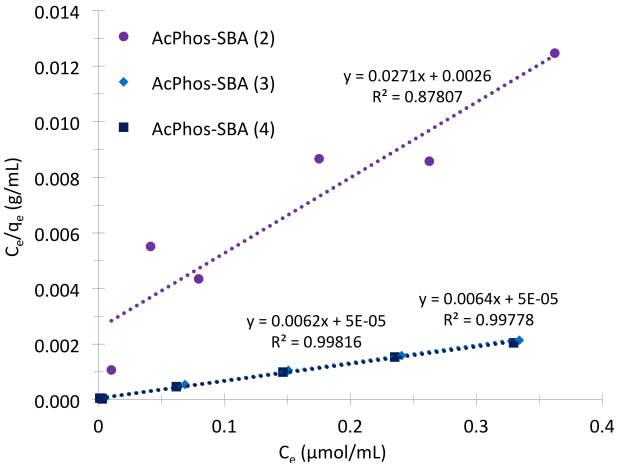

Fig. 8 Linearized Langmuir isotherm fit for U(VI) sorption from 3 M $NaNO_3$ solutions at pH 3 by AcPhos-SBA (2), (3), and (4). C_e is the equilibrium concentration of U(VI) in solution in μmol mL^{-1} and q_e is the equilibrium loading of U(VI) on the solid in μmol g^{-1}.

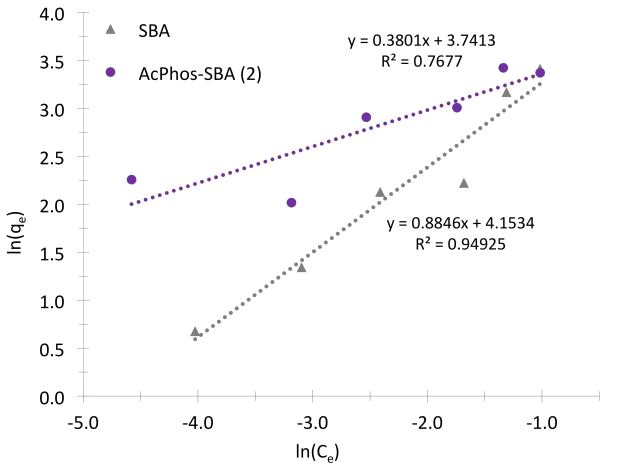

Fig. 9 Linearized Freundlich isotherm fit for U(VI) sorption from 3M $NaNO_3$ solutions at pH 3 by AcPhos-SBA (2) and non-functionalized SBA. C_e is the equilibrium concentration of U(VI) in solution in μmol mL^{-1} and q_e is the equilibrium loading of U(VI) on the solid in μmol g^{-1}.

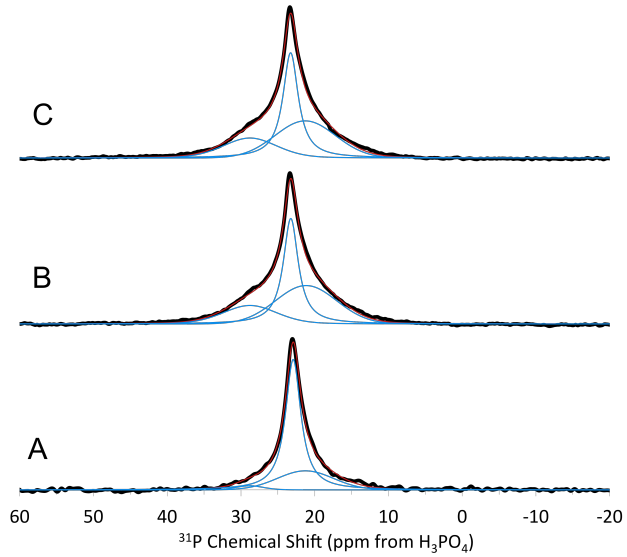

Fig. 10 Single-pulse ^{31}P NMR spectra for a) U(VI)-AcPhos-SBA (2), b) U(VI)-AcPhos-SBA (3), and c) U(VI)-AcPhos-SBA (4). Spectra were collected with no ^{1}H decoupling.

stead of the two resonances observed in the pristine and acid-washed sample spectra, there are three resonances at approximately 21, 23, and 29 ppm with respect to H_3PO_4. The resonance at 21 ppm is a very broad shoulder to the relatively sharp resonance at 23 ppm. The 23 ppm resonance is narrower than it is in the pristine and acid-washed samples' spectra. Meanwhile, the low chemical shift (≈ 15 ppm) is not present at all in the spectra for U(VI)-AcPhos-SBA samples. The changes in peak chemical shift, width, and shape are most likely due to a combination of pH 3 aqueous solution adsorbing to the silica surface, which changes the protonation environment and the hydrogen-bonding interaction observed for the pristine and acid-washed samples, as well as the sorption of U(VI) by the AcPhos ligands, as will be discussed later.

Single-pulse ^{31}P NMR spectra were also collected using continuous wave decoupling on the ^{1}H channel for AcPhos-SBA (4) pristine, acid-washed, and U(VI)-contacted. These spectra are shown in Figure S15†. Using proton decoupling slightly improved the resolution of the spectra, which aided in fitting both the ^{1}H decoupled and the non-decoupled spectra. However, it did not reveal any additional information about the structural features of the three different samples.

Table 7 Fit parameters used to deconvolute the ^{31}P spectra for the U(VI)-AcPhos-SBA samples

Material	δ_P (ppm)	FWHM (ppm)	Shape[a]	Relative Area (%)
AcPhos-SBA (2)	21.3	8.9	1	26.6
	22.9	2.5	0	70.3
	28.8	4.4	0.8	3.1
AcPhos-SBA (3)	21.3	9.6	1	41.6
	23.2	2.4	0	39.4
	28.8	8.6	0.8	19.0
AcPhos-SBA (4)	21.3	2.5	0	39.5
	23.3	2.5	0	40.1
	28.8	8.6	0.8	20.4

[a]Value gives the shape n of the pseudo-Voigt functions, $V_p(x) = nG(x) + (1-n)L(x)$, where $G(x)$ and $L(x)$ are the Gaussian and Lorentzian distribution functions, respectively.

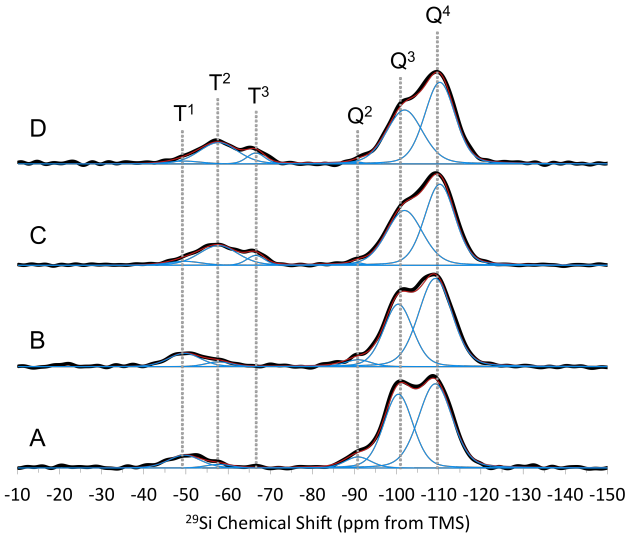

Fig. 11 Comparison of ^{29}Si{^{1}H} CP/MAS spectra of pristine a) AcPhos-SBA (1), b) AcPhos-SBA (2), c) AcPhos-SBA (3), and d) AcPhos-SBA (4). The gray dashed lines show the positions of the Q^n and T^m peaks.

Discussion

Effect of Ligand Polymerization on Functional Layer Stability. The structure and stability of the functional layer for each AcPhos-SBA can be understood by comparing their pristine and acid-washed ^{13}C{^{1}H} and ^{29}Si{^{1}H} CP/MAS NMR spectra. Contact with acidic solutions resulted in further hydrolysis of the Si−OEt groups for AcPhos-SBA (1), as evidenced by the decrease in signal amplitude in the C_7 and C_3 resonances. This change is also observed for the pristine versus acid-washed spectra for AcPhos-SBA (2) (black arrows in Figure S6†). Similar differences can be observed upon comparing the pristine spectra for AcPhos-SBA (1) and (2) with those of AcPhos-SBA (3) and (4). AcPhos-SBA (3) and (4) were synthesized with pyridine, a basic catalyst, which increases the rate of hydrolysis for the siloxane esters.[54,55] As a result, the resonances corresponding to the siloxane esters are almost completely absent in their ^{13}C{^{1}H} CP/MAS spectra. This can be interpreted as more complete hydrolysis of the Si−OEt groups during the functionalization procedure. The acid-washed spectra are very similar to the pristine spectra for both AcPhos-SBA (3) and (4), which indicates that no significant structural changes occurred upon contact with nitric acid.

The extent of reaction between the siloxane ligand and the silica surface during functionalization can be evaluated across the four different materials by comparing their ^{29}Si{^{1}H} CP/MAS NMR spectra. Figure 11 compares the pristine spectra for each material. The T populations of AcPhos-SBA (1) and (2) are dominated by the monomeric species, T^1, indicating relatively low cross-linking between ligands during functionalization. The slightly higher $T^2 : T$ ratio and slightly lower $Q^2 : Q$ and $Q^3 : Q$ ratios observed for AcPhos-SBA (2) compared to AcPhos-SBA (1) are evidence that a longer surface hydration time and a longer reflux time during functionalization resulted in slightly higher polymerization of ligands and a greater degree of functionalization. For the most part, however, there is little difference between the spectra for AcPhos-SBA (1) and (2). However, the ^{29}Si{^{1}H} CP/MAS spectra for the pristine AcPhos-SBA (3) and (4), while consistent with each other, are very different from those of AcPhos-SBA (1) and (2). The T populations of the AcPhos-SBA (3) and (4) spectra are dominated by T^2 and T^3 species. Their ^{13}C{^{1}H} CP/MAS spectra indicated more complete hydrolysis of ethoxy groups. This in turn led to a greater degree of cross-linking between ligands and/or greater reaction with surface silanols, mediated by the basic catalyst, pyridine. Additionally, compared to AcPhos-SBA (1) and (2), AcPhos-SBA (3) and (4) show reduced $Q^2 : Q$ and $Q^3 : Q$ ratios, which is consistent with reduced surface silanol content. This means that the degree of functionalization is higher for AcPhos-SBA (3) and (4) than for (1) and (2).

Comparison of the pristine and acid-washed samples reveals two general categories: the ^{29}Si spectra of AcPhos-SBA (3) and (4) do not change after contact with acid, but those of AcPhos-SBA (1) and (2) do change significantly. For both AcPhos-SBA (1) and (2), the population of T species shifts towards more T^2 and less T^1, and the $Q^3 : Q$ ratio increases, especially for AcPhos-SBA (1). Therefore, contact with acidic solutions changes the functional layer for AcPhos-SBA (1) the most, changes that of AcPhos-SBA (2) to a lesser extent, and does not measurably change those of AcPhos-SBA (3) and (4). The stability of the functional layer at the silica surface correlates with the stability of the organic layer at the silica-ligand interface. The ^{13}C{^{1}H} and ^{29}Si{^{1}H} CP/MAS NMR spectra for AcPhos-SBA (1) and (2) both indicated structural changes at the silica surface and for the carbon chains and ethoxy groups. These changes were not observed in either case for AcPhos-SBA (3) and (4), which suggests that stability of the ligand in acid is enhanced when the siloxane is completely reacted, either with neighboring siloxanes or with the silica surface.

Together the ^{13}C{^{1}H} and ^{29}Si{^{1}H} CP/MAS NMR results for the pristine and acid-washed materials reveal a trend. AcPhos-SBA (1) had the lowest degree of cross-linking between ligands and/or reaction with surface silanols. This material was also the least stable upon contact with nitric acid solutions. These results are consistent with AcPhos-SBA (1) having the lowest sorption of U(VI) from solution. AcPhos-SBA (2) demonstrated slightly higher cross-linking between ligands and/or reaction with surface silanols. As a result, it was slightly more stable to contact

with nitric acid solutions and demonstrated slightly higher sorption of U(VI). AcPhos-SBA (3) and (4) had the highest degree of cross-linking and/or reaction with surface silanols and the highest degree of stability in nitric acid solutions. These materials also demonstrated significantly enhanced sorption of U(VI), although this may be due to the formation of phosphonic acid groups, which will be discussed below.

Evidence of Formation of Phosphonic Acid Groups.

The single-pulse ^{31}P NMR spectra of pristine AcPhos-SBA (3) and (4) show evidence that hydrolysis of P−OEt groups to phosphonic acid groups, P−OH, occurred during functionalization. In addition to the resonance at 23 ppm, we observed a 15 ppm shoulder. A relatively lower chemical shift environment is consistent with increased shielding resulting from higher local electron density around the phosphorus atoms. This type of shift would only be observed for phosphonate groups acting as hydrogen bond donors through P−OH groups. Phosphonate groups acting as hydrogen-bond acceptors through the P=O group would further de-shield the phosphorus atom, causing a chemical shift in the opposite direction. The 15 ppm peak assigned to hydrolyzed, hydrogen bonding P−OH groups was only observed for AcPhos-SBA (3) and (4), which were synthesized with pyridine. Therefore, hydrolysis of the P−OEt groups is likely the result of a reaction with H_2O hydrolyzed by pyridine. The $^{13}C\{^1H\}$ CP/MAS spectra for these materials still show substantial peaks corresponding to the O=PO**C**H$_2$**C**H$_3$ carbons. Therefore, AcPhos-SBA (3) and (4) likely contain a mixture of phosphonic acid and ethyl phosphonate groups. Previous work on ethylphosphonate- and phosphonic acid-functionalized silica has shown that total hydrolysis of O=P(OEt)$_2$ to O=P(OH)$_2$ only results in a ^{31}P chemical shift of approximately -1-3 ppm in the main resonance for those materials.[31,32,51] Detecting formation of a mixture of these groups by the chemical shifting of that resonance alone is not likely. However, the presence of the lower-field chemical shift at 15 ppm in the AcPhos-SBA (3) and (4) spectra suggests that hydrolysis has occurred.

Further evidence of the formation of phosphonic acid groups can be found in the single-pulse ^{1}H NMR spectrum of AcPhos-SBA (4), shown in Figure 12. The ^{1}H spectrum shows peaks corresponding to the aliphatic carbon chain (1.3 ppm), the methylene between the phosphonate and amide groups (4.1 ppm), and the amide hydrogen (9.4). These chemical shifts are consistent with previous reports.[32,56] There is an additional peak at 17.9 ppm, indicative of a highly acidic proton. There are several reports of hydrogen-bonded phosphonic acid species giving ^{1}H giving chemical shifts in the range 10-17 ppm.[57,58] The highest chemical shifts are observed for a proton shared between two deprotonated acid groups.

The single-pulse ^{31}P NMR spectra of the U(VI)-AcPhos-SBA samples are consistent with this analysis. Bibent's study compared dried and hydrated samples of phosphonate- and phosphonic acid-functionalized SBA-15.[32] This study also observed the disappearance of the low chemical shift peak, a narrowing of the main ^{31}P peak, and the presence of shoulder peaks at close chemical shift to the central peak which broadened its base significantly. Bibent ascribed these changes to a disruption of the hydrogen-bonding network upon the adsorption of water. Water sorbed to the ligand sites will prevent or reduce hydrogen-bonding interactions between ligands, so the low chemical-shift peak at 15 ppm disappears. As a consequence, the ligands themselves become less rigid, and their increased mobility results in narrower peak shape. Bibent assigns the the different resonances observed to ligand environments with different degrees of hydration, leading to measurably different peak widths. The same argument can be used to rationalize the spectra of U(VI)-AcPhos-SBA (2), (3), and (4).

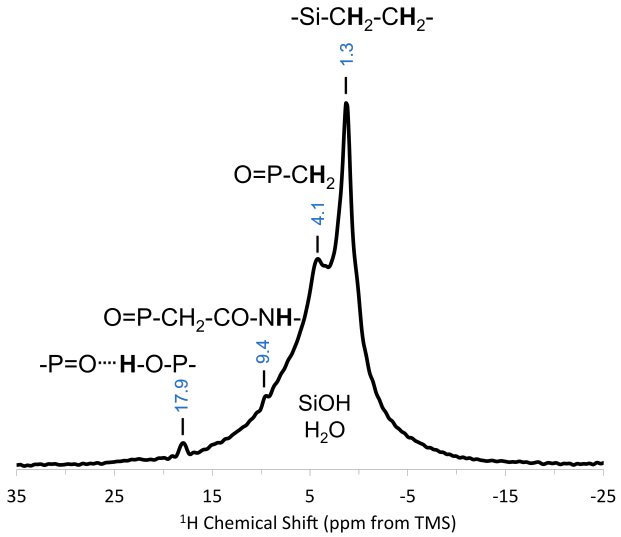

Fig. 12 Single-pulse ^{1}H NMR spectrum of AcPhos-SBA (4) AW. The resonance at 1.3 ppm is from the hydrogens on the carbon chain; the 4.1 resonance is due to hydrogens on the carbon adjacent to the phosphonate functional group; the relatively unshielded peak at 9.4 is from the amine hydrogen. The peak at 17.9 ppm likely corresponds to hydrogen atoms participating in intra-ligand hydrogen bonding.

An additional peak is observed at 29 ppm for AcPhos-SBA (2), (3), and (4). This peak is shifted approximately +6 ppm from the central peak at 23 ppm and has significant amplitude in the spectra for U(VI)-AcPhos-SBA (3) and (4). A similar chemical shift has been observed for phosphonate species bound to uranyl cations.[21] Therefore, we attribute the chemical shift at 29 ppm to AcPhos-ligands interacting with uranyl cations. These AcPhos-ligands could contain two P−OEt groups, two P−OH groups, or one of each. Further justification for this assignments is the observation that the amplitude of the 29 ppm resonance is higher for the U(VI)AcPhos-SBA (3) and (4) spectra than it is for the U(VI)-AcPhos-SBA (2) spectrum (Figure 10), and it is known from the batch contact experiments that AcPhos-SBA (3) and (4) sorb significantly more U(VI) under these conditions than AcPhos-SBA (2).

Influence of Functionalization Procedure on U(VI) Sorption.

The three different functionalization methods tested (AcPhos-SBA (3) and (4) were synthesized using the same method) yielded significantly different U(VI) sorption properties. AcPhos-SBA

(3) and (4) demonstrated significantly different U(VI) sorption isotherms than AcPhos-SBA (2). The data for AcPhos-SBA (3) and (4) was well-described by the Langmuir adsorption isotherm. For these materials, the average sorption capacity measured was 160 ± 2 μmol g^{-1} silica, and the average K_{eq} was 117 ± 32 mL μmol^{-1}. In contrast, the data for AcPhos-SBA (2) was described equally well by the Langmuir and Freundlich isotherm models, but not very well by either of them. The Langmuir fit for AcPhos-SBA (2) U(VI) isotherm data yielded a sorption capacity of 37 ± 7 μmol g^{-1} and a K_{eq} of 11 ± 5 μmol^{-1}. The different isotherm behavior is consistent with different chemical processes occurring in the extraction of U(VI) by each type of material. This difference may be the result of an ion-exchange extraction mechanism occurring on hydrolyzed AcPhos ligands in AcPhos-SBA (3) and (4) versus an interaction between a neutral ligand and U(VI) for the non-hydrolyzed ligands on AcPhos-SBA (2). The interaction between a negatively charged phosphonic acid species and cationic uranyl would result in a higher stability constant than the interaction between uranyl and a neutral ligand, as is observed here.

The Langmuir sorption isotherm model assumes a single type of binding site characterized by one binding energy, which is uniform across the surface and independent of the concentration of the analyte sorbed to the surface. In contrast, the Freundlich sorption isotherm model accounts for a more complex interaction, with more than one type of binding site and a distribution of binding energies. We observe that the U(VI) sorption isotherm for non-functionalized SBA-15 is described well by the Freundlich model. This model is consistent with the amorphous silica surface, which presents a distribution of densities and geometries of surface silanols, the primary binding sites for uranyl cations. In contrast, the Langmuir model describes the shape of the U(VI) sorption isotherm for AcPhos-SBA (3) and (4). A strong, electrostatic interaction between phosphonate anions and a uranyl cations would manifest as a single type of binding interaction dominating the sorption isotherm, resulting in a Langmuir fit to the data.

The U(VI) sorption isotherm for AcPhos-SBA (2) was not described particularly well by either the Langmuir or Freundlich models, which is evidence that a more complex sorption environment exists between uranyl cations and AcPhos-SBA (2). In our previous work,[21] we observed that the sorption of U(VI) on diethylphosphonate (DPTS)-functionalized SBA-15 from pH 4 nitric acid solutions was described slightly better by the Freundlich model than the Langmuir model. Combined with evidence from NMR spectroscopy, observation of the Freundlich sorption isotherm led us to believe that the uranyl ions were complexed to both ligands and surface silanols. It is likely that sorption of U(VI) to AcPhos-SBA (2) contains a similar extraction mechanism involving both phosphonate ligands and surface silanols. This mechamism is consistent with the lack of hydrolyzed phosphonate groups for AcPhos-SBA (2), as evidenced by a single resonance in the ^{31}P NMR spectrum, and also by the higher surface silanol content, as evidenced by higher $Q^2 : Q$ and $Q^3 : Q$ ratios compared to AcPhos-SBA (3) and (4). For AcPhos-SBA (3) and (4) the surface silanol content is decreased, and the presence of P−OH groups makes stronger, electrostatic binding interactions accessible, resulting in a more uniform, Langmuir-type interaction between U(VI) and the surface.

Higher U(VI) sorption is also correlated with higher stability of the functional layer. Formation of phosphonic acid groups during functionalization accounts for the different uptake observed for AcPhos-SBA (3) and (4) compared to (1) and (2). However, the presence of phosphonic acid groups cannot account for the difference in sorption observed for AcPhos-SBA (2) compared to (1), since no hydrolysis of ethylphosphonate was observed for these samples. Despite its low U(VI) sorption capacity, AcPhos-SBA (2) did sorb measurable amounts of uranyl from nitric acid solutions above pH 3, but AcPhos-SBA (1) did not. The lack of any measurable sorption of U(VI) on AcPhos-SBA (1) may be due to the degradation of its functional layer, as evidenced by changes in its ^{29}Si NMR spectra. Ultimately increased stability resulted in greater uptake of U(VI) from solution.

Comparison of Ligand Density for AcPhos-SBA Materials.

^{31}P-^{31}P homonuclear dipolar coupling measurements were made to compare the average density of AcPhos ligands on the silica surface as well as their degree of polymerization for each material. The strength of dipolar coupling depends on the number and proximity of nearby spins. The sum of all pairwise spin dipolar coupling constants, $\sum_{j<k} b_{jk}^2$, is related to the distance between each spin, r_{jk} through:

$$\sum_{j,k} b_{jk}^2 = h^2\gamma^2\left(\frac{\mu_0}{4\pi}\right)\cdot\sum_{j,k}\frac{1}{r_{jk}^6} \qquad (2)$$

where b_{jk} is in Hz, γ is the gyromagnetic ratio for ^{31}P in Hz T^{-1}, and μ_0 is the vacuum permeability constant. Therefore, a "denser" ligand layer will demonstrate stronger ^{31}P-^{31}P coupling. This manifests as a greater difference in signal amplitude, ΔS, and a steeper rise in the plot of $\Delta S/S_0$ versus NT_r. AcPhos-SBA (1) had the lowest $\sum_{j<k} b_{jk}^2 = (1.9 \pm 0.1) \times 10^5 Hz^2$ of all four materials. This is consistent with its lower T^2 and T^3 peak intensities compared with the other materials. A longer surface hydration and refluxing time resulted in slightly higher cross-linking between ligands for AcPhos-SBA (2). This material also had a higher $\sum_{j<k} b_{jk}^2 = (2.64 \pm 0.03) \times 10^5 Hz^2$. AcPhos-SBA (3) and (4), which had a much higher degree of cross-linking based on their ^{29}Si{^{1}H} CP/MAS spectra, demonstrated similarly high dipolar coupling interactions, with $\sum_{j<k} b_{jk}^2$ values of $(2.93 \pm 0.07) \times 10^5$ and $(2.45 \pm 0.09) \times 10^5$, respectively. That the difference in dipolar coupling strength between the AcPhos-SBA (2) and (4) samples is not significant is surprising, given the vast differences in the T^2 and T^3 Si populations. However, this may constitute evidence that the T^2 and T^3 chemical shifts are due not only to a higher degree of ligand polymerization, but also due to a higher degree of reaction with the surface, that is, formation of R−Si−(OX), where X is Si from the silica substrate rather than from a neighboring siloxane. The addition of pyridine catalyzes hydrolysis of siloxane groups, but would also tend to deprotonate surface silanols. Therefore, the rate of polymerization and the rate of condensation to the surface are both affected by the addition of pyridine.

The two different phosphorus chemical shift environments

present in AcPhos-SBA (4) demonstrate significantly different ^{31}P-^{31}P dipolar coupling strength. The parabolic rise of the 15 ppm resonance is steeper than that of the 23 ppm resonance. This results in a higher $\sum_{j,k} b_{jk}^2$ value of $(5.7 \pm 0.3) \times 10^5 Hz^2$ compared to $(2.45 \pm 0.09) \times 10^5 Hz^2$ for the 23 ppm peak, which corresponds to a higher overall ligand density for this phosphorus environment.

In previous work, we describe a model of the modified silica surface based on the crystal structure of β-cristobalite.[21,59] Assuming ligands are rigid on the timescale of the NMR experiment, two phosphorus atoms that are part of a pair of cross-linked ligands (i. e. R−Si−O−Si−R, where R is the AcPhos ligand) would be spaced approximately 3.0 Å apart.[60] If no cross-linking between ligands occurred, and only exposed silanols were functionalized, phosphorus atoms would be spaced approximately 5.0 Å apart, with a maximum of six nearest neighbors. Using Equation 2, the expected $\sum_{j,k} b_{jk}^2$ values can be calculated for a given number of ^{31}P spins at a fixed distance apart. For example, "monomeric" functionalization, resulting in six nearest neighbors at a distance of 5 Å would yield $\sum_{j,k} b_{jk}^2 = 1.49 \times 10^5 Hz^2$ (Figure 13). A dimerized ligand pair, where there is one nearest neighbor at a distance of 3.0 Å yields $\sum_{j,k} b_{jk}^2 = 5.31 \times 10^5 Hz^2$, which is very similar to the value observed for the 15 ppm peak in the AcPhos-SBA (4) sample. The slightly higher $\sum_{j,k} b_{jk}^2$ value observed for the 15 ppm peak of AcPhos-SBA (4) can be explained by the presence of 1 or 2 other phosphonate groups at a distance of 5.0 Å, which would yield $\sum_{j,k} b_{jk}^2$ values between $5.56 \times 10^5 Hz^2$ and $5.81 \times 10^5 Hz^2$ (Figure 13). These values match that observed for the 15 ppm peak, $\sum_{j,k} b_{jk}^2 = (5.7 \pm 03) \times 10^5 Hz^2$ within the uncertainty of the fit. Combined with single pulse ^{31}P and ^{1}H NMR, the DQ-DRENAR data shows that the phosphorus chemical environment corresponding to the 15 ppm peak corresponds to ligand pairs that dimerized at their alkoxysilane anchors during functionalization, were hydrolyzed to contain one or more P−OH groups upon contact with pyridine, and are involved in hydrogen-bonding interactions between P−OH groups. The closer proximity of hydrolyzed phosphonate groups suggest that hydrogen bonding may occur prior to or during surface condensation reactions, suggesting that inter-ligand hydrogen bonding may play a role in monolayer formation. This could be a rich area of future study.

Conclusion

Three different functionalization methods were used to modify SBA-15 rods with an acetamide phosphonate ligand, and the materials were evaluated for their ability to uptake U(VI) from nitric acid solutions and for the resilience of the functional layer to contact with nitric acid during these experiments. Increasing the hydration time and refluxing time during functionalization resulted in marginal increases in the cross-linking of ligands, which improved its stability in pH 3 nitric acid. The addition of pyridine as a basic catalyst during functionalization was found to increase hydrolysis of ethoxysilane groups, which provided for greater reactivity between ligands and between the ligands and the silanol surface. ^{13}C{^{1}H} and ^{29}Si{^{1}H} showed that materials synthesized with pyridine were more stable to contact with 3 M $NaNO_3$ adjusted to pH 3 than those synthesized without it. Additionally, they showed increased sorption under all conditions tested. Measurement of U(VI) isotherms revealed significantly different sorption behavior, including a stronger interaction between U(VI) and the AcPhos ligand for materials synthesized with pyridine.

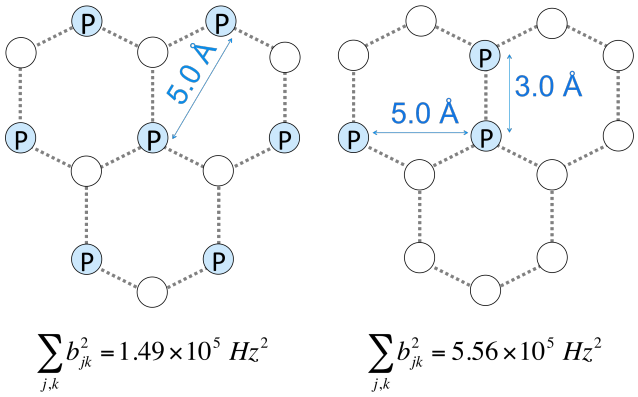

Fig. 13 Diagram showing the model based on the 111 surface of β-cristobalite. Left: model for low ligand cross-linking, resulting in âĂIJmonomericâĂİ functionalization. Right: model for higher ligand cross-linking, showing a mixture of dimers and monomers.

Additionally, single-pulse ^{31}P and ^{1}H NMR showed evidence that pyridine had partially hydrolyzed ethyl phosphonate to phosphonic acid groups. Consistent with previous reports, a lower chemical shift peak was observed at 15 ppm in the ^{31}P NMR spectra only for materials synthesized with pyridine, and this peak was assigned to hydrolyzed phosphonates involved in hydrogen bonding interactions. The DQ-DRENAR method was used to compare the strength of ^{31}P-^{31}P dipolar coupling for each of the materials synthesized. These measurements revealed that chemical environments corresponding to hydrolyzed, deprotonated phosphonic acid ligands engaged in hydrogen bonding interactions demonstrate higher dipolar coupling interactions and are therefore characterized by a higher average ligand density than the free AcPhos ligands.

Single-pulse ^{31}P NMR spectra collected for U(VI)-AcPhos-SBA samples revealed that the combination of sorption of uranyl cation to the AcPhos ligand and of water to the functional layer resulted in disruption of the hydrogen bonding interaction between ligands. Additionally, a +6 ppm shift from the main peak at 23 ppm was observed for AcPhos ligands bound to U(VI).

We have shown that dipolar coupling measurement by NMR spectroscopy is very useful for studying self-assembledmonolayers on silica substrates, especially for ligands containing ^{31}P, which is naturally abundant. The process of functionalization is complex and differs based on the precise conditions used. The DQ-DRENAR method provides an elegant and fast way to measure the distribution of ligands on a surface.

Acknowledgments

The authors would like to acknowledge the contributions of Annie B. Kersting and the Glenn T. Seaborg Institute at Lawrence Livermore National Laboratory. They would also like to acknowl-

edge Professor Jeff Long and Doug Reed of the University of California, Berkeley for the nitrogen adsorption isotherm measurements. This work was supported by the National Nuclear Security Administration (NNSA) under the Stewardship Science Academic Alliance Program, award number DE-NA0001978. This work was performed under the auspices of the U.S. Department of Energy by Lawrence Livermore National Laboratory under Contract DE-AC52-07NA27344. E.C.U. was supported by a National Science Foundation Graduate Research Fellowship under Grant No. DGE 1106400. Portions of this work were performed at Lawrence Berkeley National Laboratory of the U.S. Department of Energy under Contract No. DE-AC02-05-CH11231.

References

1 J. Ren and H. Eckert, *Angewandte Chemie (International Ed.)*, 2012, **51**, 12888–12891.

2 J. Ren and H. Eckert, *Journal of Chemical Physics*, 2013, **138**, 1–16.

3 E. P. Horwitz, M. L. Dietz, D. M. Nelson, J. J. LaRosa and W. D. Fairman, *Analytica Chimica Acta*, 1990, **238**, 263–271.

4 E. P. Horwitz, M. L. Dietz, R. Chiarizia and H. Diamond, *Analytica Chimica Acta*, 1992, **266**, 25–37.

5 P. Horwitz, R. Chiarizia, M. L. Dietz, H. Diamond and D. M. Nelson, 1993, **281**, 361–372.

6 A. Bhattacharyya, P. K. Mohapatra and V. K. Manchanda, *Journal of Chromatography A*, 2006, **1123**, 26–30.

7 Y. Wei, M. Kumagai, Y. Takashima, G. Modolo and R. Odoj, *Nuclear Technology*, 2000, **132**, 413–423.

8 A. Bhattacharyya, P. K. Mohapatra and V. K. Manchanda, *Solvent Extraction and Ion Exchange*, 2007, **25**, 27–39.

9 Q. Yang, L. Yang, J. Liu, Y. Li and C. Li, *Chemistry of Materials*, 2005, **17**, 3019–3024.

10 D. Mauder, D. Akcakayiran, S. B. Lesnichin, G. H. Findenegg and I. G. Shenderovich, *Journal of Physical Chemistry C*, 2009, **113**, 19185–19192.

11 P. Wang, L. Zhao, R. Wu, H. Zhong, H. Zou, J. Yang and Q. Yang, *The Journal of Physical Chemistry C*, 2009, **113**, 1359–1366.

12 P. N. Nesterenko, O. S. Zhukova, O. A. Shpigun and P. Jones, *Journal of Chromatography A*, 1998, **813**, 47–53.

13 R. J. P. Corriu, L. Datas, Y. Guari, A. Mehdi, C. Reyé and C. Thieuleux, *Chemical Communications*, 2001, 763–764.

14 P. J. Lebed, K. de Souza, F. Bilodeau, D. Larivière and F. Kleitz, *Chemical Communications*, 2011, **47**, 11525–7.

15 P. J. Lebed, J.-d. Savoie, J. Florek, F. Bilodeau, D. Larivière and F. Kleitz, *Chemistry of Materials*, 2012, **24**, 4166–4176.

16 Y.-L. Wang, L. Zhu, B.-L. Guo, S.-W. Chen and W.-S. Wu, *New Journal of Chemistry*, 2014, **38**, 3853.

17 J. L. Vivero-Escoto, M. Carboni, C. W. Abney, K. E. DeKrafft and W. Lin, *Microporous and Mesoporous Materials*, 2013, **180**, 22–31.

18 W. Zhang, G. Ye and J. Chen, *Journal of Materials Chemistry A*, 2013, 3–6.

19 L.-Y. Yuan, Y.-L. Liu, W.-Q. Shi, Y.-L. Lv, J.-H. Lan, Y.-L. Zhao and Z.-F. Chai, *Dalton Transactions*, 2011, **40**, 7446–53.

20 X. Wang, L. Yuan, Y. Wang, Z. Li, J. Lan, Y. Liu, Y. Feng, Y. Zhao, Z. Chai and W. Shi, *Science China Chemistry*, 2012, **55**, 1705–1711.

21 E. C. Uribe, H. E. Mason, J. A. Shusterman, A. Bruchet and H. Nitsche, *Dalton Trans.*, 2016, 10447–10458.

22 O. A. Dudarko, C. Gunathilake, N. P. Wickramaratne, V. V. Sliesarenko, Y. L. Zub, J. Górka, S. Dai and M. Jaroniec, *Colloids and Surfaces A: Physicochemical and Engineering Aspects*, 2015, **482**, 1–8.

23 G. E. Fryxell, H. Wu, Y. Lin, W. J. Shaw, J. C. Birnbaum, J. C. Linehan, Z. Nie, K. Kemner and S. Kelly, *Journal of Materials Chemistry*, 2004, **14**, 3356.

24 G. E. Fryxell, S. V. Mattigod, Y. Lin, H. Wu, S. Fiskum, K. Parker, F. Zheng, W. Yantasee, T. S. Zemanian, R. S. Addleman, J. Liu, K. Kemner, S. Kelly and X. Feng, *Journal of Materials Chemistry*, 2007, **17**, 2863.

25 J. C. Birnbaum, B. Busche, Y. Lin, W. J. Shaw and G. E. Fryxell, *Chemical Communications*, 2002, 1374–1375.

26 W. Yantasee, Y. Lin, G. E. Fryxell, B. J. Busche and J. C. Birnbaum, *Separation Science and Technology*, 2003, **38**, 3809–3825.

27 W. Yantasee, G. E. Fryxell, R. S. Addleman, R. J. Wiacek, V. Koonsiripaiboon, K. Pattamakomsan, V. Sukwarotwat, J. Xu and K. N. Raymond, *Journal of Hazardous Materials*, 2009, **168**, 1233–8.

28 G. E. Fryxell, Y. Lin, S. Fiskum, J. C. Birnbaum, H. Wu, K. Kemner and S. Kelly, *Environmental Science & Technology*, 2005, **39**, 1324–1331.

29 G. E. Fryxell, *Actinide-Specific Interfacial Chemistry of Monolayer Coated Mesoporous Ceramics*, 2001.

30 T. Parsons-Moss, *UC Berkeley Ph.D. Dissertation*, 2014.

31 Y.-c. Pan, H.-h. G. Tsai, J.-c. Jiang, C.-c. Kao, T.-l. Sung, P.-j. Chiu, D. Saikia, J.-h. Chang and H.-m. Kao, *Journal of Physical Chemistry C*, 2012, **116**, 1658–1669.

32 N. Bibent, T. Charpentier, S. Devautour-Vinot, A. Mehdi, P. Gaveau, F. Henn and G. Silly, *European Journal of Inorganic Chemistry*, 2013, 2350–2361.

33 J. Shusterman, H. Mason, A. Bruchet, M. Zavarin, A. B. Kersting and H. Nitsche, *Dalton Transactions*, 2014, **43**, 16649–16658.

34 A. Sayari, B. H. Han and Y. Yang, *Journal of the American Chemical Society*, 2004, **126**, 14348–14349.

35 L. C. Sander and S. A. Wise, *Anal. Chem.*, 1995, **67**, 3284–3292.

36 S. Brunauer, P. H. Emmett and E. Teller, *Journal of the American Chemical Society*, 1938, **60**, 309–319.

37 E. P. Barrett, L. G. Joyner and P. P. Halenda, *Journal of the American Chemical Society*, 1951, **73**, 373–380.

38 D. L. Rabenstein and T. L. Sayer, *Journal of Magnetic Resonance*, 1976, **24**, 27–39.

39 M. Magi, E. Lippmaa, a. Samoson, G. Engelhardt and a. R. Grimmer, *The Journal of Physical Chemistry*, 1984, **88**, 1518–1522.

40 W. Li, W. Xu, J. B. Parise and B. L. Phillips, *Geochimica et Cosmochimica Acta*, 2012, **85**, 289–301.
41 J. P. Yesinowski and H. Eckert, *Journal of the American Chemical Society*, 1987, **109**, 6274–6282.
42 K. S. W. Sing, D. H. Everett, R. A. W. Haul, L. Moscou, R. A. Pierotti, J. Rouquérol and T. Siemieniewska, *Pure and Applied Chemistry*, 1985, **57**, 603–619.
43 V. Antochshuk and M. Jaroniec, *Chemistry of Materials*, 2000, **12**, 2496–2501.
44 J. A. Shusterman, H. E. Mason, J. Bowers, A. Bruchet, E. C. Uribe, A. B. Kersting and H. Nitsche, *Applied Materials & Interfaces Interfaces*, 2015, **7**, 20591–20599.
45 A. Boutin, B. Coasne, A. H. Fuchs, A. Galarneau and F. Di Renzo, *Langmuir*, 2012, **28**, 9526–9534.
46 D. W. Sindorf and G. E. Maciel, *Journal of the American Chemical Society*, 1980, **102**, 7607.
47 C. C. Liu and G. E. Maciel, *Journal of the American Chemical Society*, 1996, **118**, 5103–5119.
48 D. W. Sindorf and G. E. Maciel, *Journal of the American Chemical Society*, 1981, **103**, 4263–4265.
49 X. Feng, G. E. Fryxell, L.-Q. Wang, A. Y. Kim, J. Liu and K. M. Kemner, *Science*, 1997, **276**, 923–926.
50 A. Aliev, D. L. Ou, B. Ormsby and A. C. Sullivan, *Journal of Materials Chemistry*, 2000, **10**, 2758–2764.
51 I. V. Melnyk, M. Fatnassi, T. Cacciaguerra, Y. L. Zub and B. Alonso, *Microporous and Mesoporous Materials*, 2012, **152**, 172–177.
52 Y. J. Lee, B. Bingo, T. Murakhtina, D. Sebastiani, W. H. Meyer, G. Wegner and H. W. Spiess, *Journal of Physical Chemistry B*, 2007, **111**, 9711–9721.
53 S. W. Yang, D. C. Doetschman, J. T. Schulte, J. B. Sambur, C. W. Kanyi, J. D. Fox, C. O. Kowenje, B. R. Jones and N. D. Sherma, *Microporous and Mesoporous Materials*, 2006, **92**, 56–60.
54 B. Arkles, J. Steinmetz, J. Zazyczny and P. Mehta, *Journal of Adhesion Science and Technology*, 1992, **6**, 193–206.
55 T. Martin, A. Galarneau, F. D. Renzo, D. Brunel, F. Fajula, S. Heinisch, G. Cretier and J.-L. Rocca, *Chemistry of Materials*, 2004, **16**, 1725–1731.
56 L. T. Byrne, V. Ferro, S. Stevenson and R. V. Stick, 1994, **32**, 749–752.
57 J. W. Blanchard, T. L. Groy, J. L. Yarger and G. P. Holland, *Journal of Physical Chemistry C*, 2012, **116**, 18824–18830.
58 R. K. Harris, P. Jackson, L. H. Merwin, B. J. Say and G. Hï£ıgele, *Journal of the Chemical Society, Faraday Transactions 1*, 1988, **84**, 3649.
59 I.-s. Chuang and G. Maciel, *The Journal of Physical Chemistry B*, 1997, **101**, 3052–3064.
60 J. J. Pluth, J. V. Smith and J. Faber, *Journal of Applied Physics*, 1985, **57**, 1045–1049.